Taylor & Francis
Taylor & Francis Group

Computer Methods in Biomechanics and Biomedical Engineering

ISSN: 1025-5842 (Print) 1476-8259 (Online) Journal homepage: https://www.tandfonline.com/loi/gcmb20

An image-based method to measure joint deformity in inflammatory arthritis: development and pilot study

Travis F. Henchie, Ellen M. Gravallese, Todd L. Bredbenner & Karen L. Troy

To cite this article: Travis F. Henchie, Ellen M. Gravallese, Todd L. Bredbenner & Karen L. Troy (2019): An image-based method to measure joint deformity in inflammatory arthritis: development and pilot study, Computer Methods in Biomechanics and Biomedical Engineering, DOI: 10.1080/10255842.2019.1607315

To link to this article: https://doi.org/10.1080/10255842.2019.1607315

COMPUTER METHODS IN BIOMECHANICS AND BIOMEDICAL ENGINEERING
https://doi.org/10.1080/10255842.2019.1607315

An image-based method to measure joint deformity in inflammatory arthritis: development and pilot study

Travis F. Henchie[a]*, Ellen M. Gravallese[b], Todd L. Bredbenner[c] and Karen L. Troy[a]

[a]Department of Biomedical Engineering, Worcester Polytechnic Institute, Worcester, Massachusetts, USA; [b]Division of Rheumatology, University of Massachusetts Memorial Medical Center and University of Massachusetts Medical School, Worcester, Massachusetts, USA; [c]Department of Mechanical and Aerospace Engineering, University of Colorado Colorado Springs, Colorado Springs, Colorado, USA

ABSTRACT

Quantifying joint deformity in people with rheumatoid (RA) and psoriatic arthritis (PsA) remains challenging. Here, we demonstrate a new method to measure bone erosions and abnormal periosteal growths, based on the difference between a predicted healthy and actual diseased joint surface. We optimized the method by creating and measuring artificial bone erosions and growths. Then we measured 46 healthy and diseased patient surfaces. We found average sensitivity errors of $\leq$0.27 mm when measuring artificial erosions and growths. Patients had significantly more bone erosion than healthy subjects. Surface based outcomes are a novel way to interpret and quantify bone changes in PsA and RA.

ARTICLE HISTORY
Received 30 August 2018
Accepted 10 April 2019

KEYWORDS
Coherent point drift; HRpQCT; CT; imaging; inflammatory arthritis; MCP

1. Introduction

Psoriatic arthritis (PsA) and rheumatoid arthritis (RA) are chronic inflammatory diseases occurring in patients with autoimmune disorders and psoriasis (Gladman, 2009; Cantini et al., 2010; Schett and Gravallese, 2012). A combination of mechanical stress and inflammation in individuals with PsA results in the formation of periosteal bone growth (osteophytes or enthesophytes) at tendon/ligament insertion sites, and articular erosions within the joints (Frank, 1998; Cantini et al., 2010; Simon et al., 2015). Erosion formation typically occurs in early disease at the proximal enthesis, but in later stages, spur formation occurs at the distal end of the ligament attachment site (McGonagle et al., 2015). The frequency and size of the abnormalities and the number of affected joints are associated with poor clinical outcomes (Schett and Gravallese, 2012). Some individuals exhibit extremely destructive and disfiguring forms of the disease with erosions and periosteal bone formation leading to disability (Gladman et al., 1987; Duarte et al., 2012). The metacarpophalangeal joints of the hand are common areas for bone changes. Because these changes are irreversible (Solomon et al., 2017), earlier detection and prevention may lead to improved patient care.

Radiographic imaging is the most common modality to identify and assess features of both RA and PsA including erosions, joint space narrowing, bony proliferation and formation (Rahman et al., 2001; Ory et al., 2005). However, radiography has low sensitivity for the detection of degenerative features in early disease stages, and these features are often poorly defined due to the progression of periosteal bone formation adjacent to erosions (Ory et al., 2005). Computed tomography (CT), magnetic resonance imaging (MRI) and ultrasound imaging are gaining clinical popularity. These technologies are capable of detecting early stages of disease and monitoring joint changes during disease progression with greater sensitivity than that of plain radiographs (Ostergaard, 2005; Boutry et al., 2007; Baillet et al., 2011; Huizinga et al., 2011; Zayat et al., 2014). Outcome Measures in Rheumatoid Arthritis Clinical Trials (OMERACT) has developed Psoriatic Arthritis Magnetic Resonance Imaging Score (PsAMRIS) for the evaluation of joint damage in PsA in hands using MRI (Østergaard et al., 2009; Boyesen

CONTACT Karen L. Troy ktroy@wpi.edu Department of Biomedical Engineering, Worcester Polytechnic Institute, 100 Institute Road, Worcester, MA 01609, USA
*Current affiliation: Boston Scientific Corporation, Marlborough, Massachusetts, USA.
Submitted to: Computer Methods in Biomechanics and Biomedical Engineering Revision 1: March 8, 2019.
Supplemental data for this article can be accessed at https://doi.org/10.1080/10255842.2019.1607315.

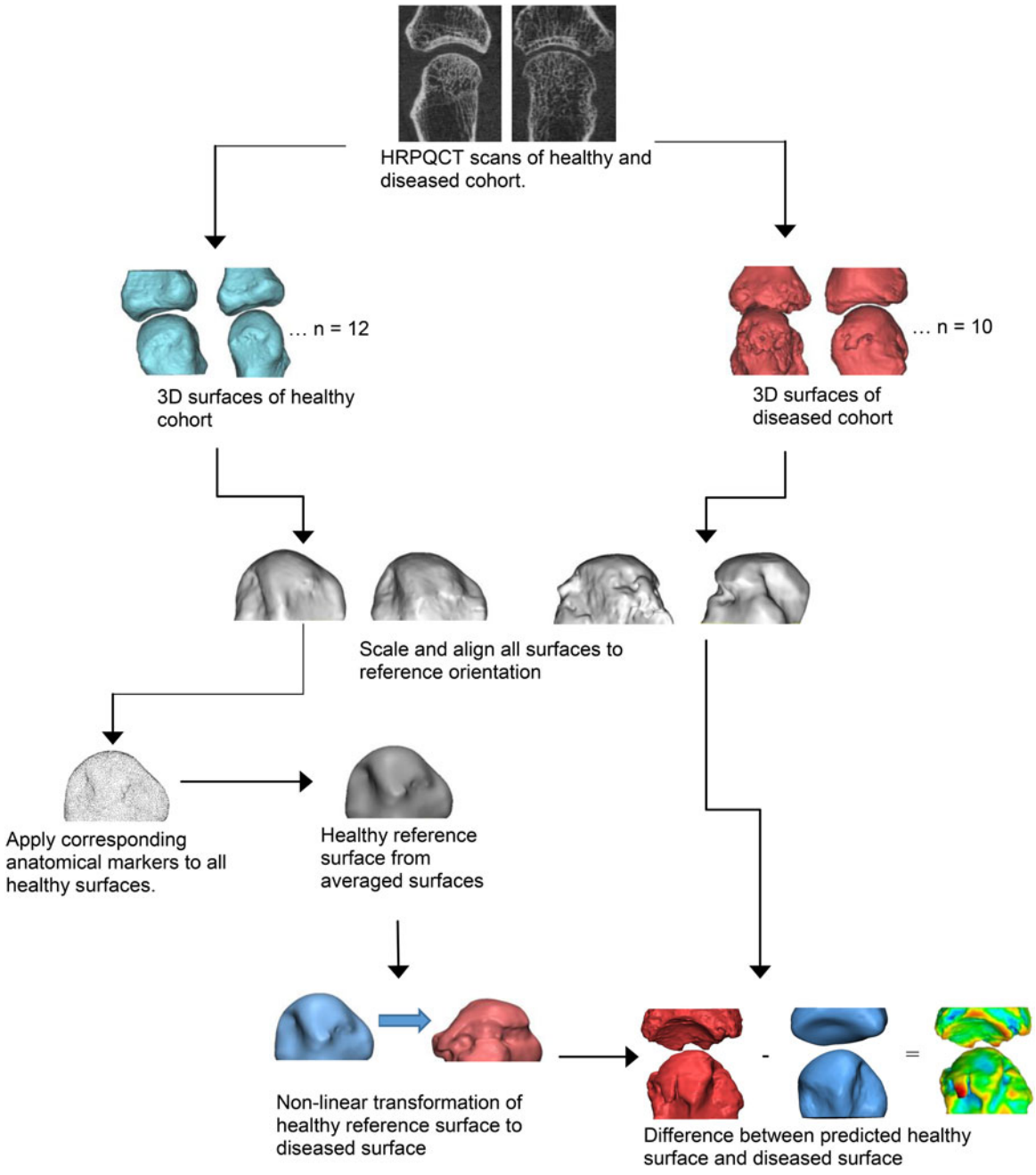

Figure 1. Illustration of algorithm overview as describing the dependent chronological order of events to estimate a healthy bone surface from a diseased surface.

et al., 2011) evaluating multiple joints and patient disability. Similarly, Rheumatoid Arthritis Magnetic Imaging Score (RAMRIS) exists for evaluating RA (Haavardsholm et al., 2005; Ostergaard, 2005).

High-resolution peripheral computed tomography (HRpQCT) is a low radiation dose imaging technique with the ability to assess three-dimensional (3D) bone structure in the peripheral bones with a voxel resolution range of 63 - 246 µm (SCANCO Medical. XtremeCT, 2017). Although it remains primarily a research tool, HRpQCT is gaining popularity and clinical accessibility as a means to quantify bone degradation in RA patients, with multiple studies reporting on the visual analysis of erosion number and size, and user reliability (Fouque-Aubert et al., 2010; Stach et al., 2010; Burghardt et al., 2013; Nishiyama and Shane, 2013; Kocijan et al., 2014; Paccou et al., 2014). Several publications report positive results for semi-automated algorithms capable of segmenting erosions in patients with RA from cortical interruptions in the

bone surface (Duryea et al., 2008; Burghardt et al., 2013; Töpfer et al., 2014; Cervinka et al., 2015; Duryea et al., 2016; Peters et al., 2017). These methods show good results in erosion identification and quantification in images where erosions are easily defined. However, current algorithms require user intervention to identify an erosion by manually locating seed points or assisting in segmentation. Additionally, quantifying erosion geometry presents methodological challenges because it depends on the subjective estimation of the original (missing) bone surface. This becomes inaccurate in severely damaged joint areas, or when periosteal bone develops adjacent to erosions. Similar challenges are encountered when measuring periosteal bone growths.

Quantifying deformities of the bone at the articular joint surface is critical to understanding the extent of disability as a result of skeletal deformity. Thus, a goal of this research is to take advantage of HRpQCT to develop objective measurement methods that have been previously unavailable. Patient outcomes may be improved with more sensitive and less subjective measures of joint damage. The long-term goal is to improve the treatment of arthritic diseases by providing accurate, objective and clinically relevant diagnostic tools that may be used to quantify and predict disease progression.

Here, we present a new approach using HRpQCT images to detect and quantify diseased bone surface comprised of both erosions and periosteal bone growth. The algorithm is designed to predict the prior healthy bone surface from the geometry of a diseased bone surface using a probabilistic approach and a set of healthy bone surfaces as a reference. We assessed the performance of the algorithm by creating artificial erosions and periosteal bone growths. Finally, we applied the algorithm to images from a pilot group of patients with PsA and RA. We report potentially clinically relevant outcome measures between diseased cohorts and a healthy cohort, highlighting the algorithm's capability in objectively detecting diseased bone surface in a repeatable manner.

2. Methods

2.1. Subjects and image acquisition

In vivo images of the second metacarpophalangeal (MCP) joint, including the metacarpal head and phalangeal base, were acquired in pilot cohorts of healthy subjects, patients with RA and patients with PsA using HRpQCT (XtremeCT, Scanco Medical AG, Brüttisellen, Switzerland). Images were acquired on the predominantly affected hand of 17 RA patients (age 61 ± 18 years, 12 females, 5 males) and 17 PsA subjects (age 60 ± 18 years, 7 females, 10 males) and enrolled from the Rheumatology Division at University of Massachusetts Memorial Medical Center (UMMMC). Each patient had radiographic confirmation of erosions and periosteal bone formation on the imaged hand. The healthy cohort consisted of 12 subjects (age 52 ± 14 years, 7 females, 5 males), devoid of known immuno-deficiencies. Each image set consisted of 330 slices with 82 µm isotropic voxel size, encompassing a length of 27 mm spanning the second MCP joint. The total scan time was 8.5 minutes, and the associated effective radiation dose was 9 µSv. During the scan, the hands and fingers were stabilized using a combination of the manufacturer-supplied carbon fiber cast and pieces of foam packed around the hand. This study was approved by the Institutional Review Boards at Worcester Polytechnic Institute and the University of Massachusetts Medical School. All participants provided written informed consent prior to participation.

2.2. Surface transformation algorithm

2.2.1. Overview

The algorithm to calculate bone surface abnormalities is summarized in Figure 1. It consists of the following steps: (1) the phalangeal base and metacarpal head are segmented from the HRpQCT images and converted into 3 D surface meshes; (2) Corresponding anatomical points are applied to the cohort of healthy surfaces; (3) A generic healthy reference surface of the MCP joint is generated by averaging the corresponding points on the healthy surfaces; (4) The healthy reference surface is non-rigidly transformed to the shape of each diseased patient surface, while retaining the original healthy features; (5) periosteal bone growths and erosions are defined as regions where the surface of the diseased bone deviates from the transformed healthy bone surface.

2.2.2. Three-dimensional surface generation

HRpQCT images were converted to three-dimensional (3D) surface meshes (Mimics & 3Matic, Materialise NV, Leuven, Belgium, 2015) in preparation for surface-to-surface registration. To accomplish this, a binomial blur filter was first applied to each CT slice to reduce noise. Next, voxels representing bone were identified using a fixed density threshold of 0.41 g/cm^3. The internal trabecular region was excluded in this analysis.

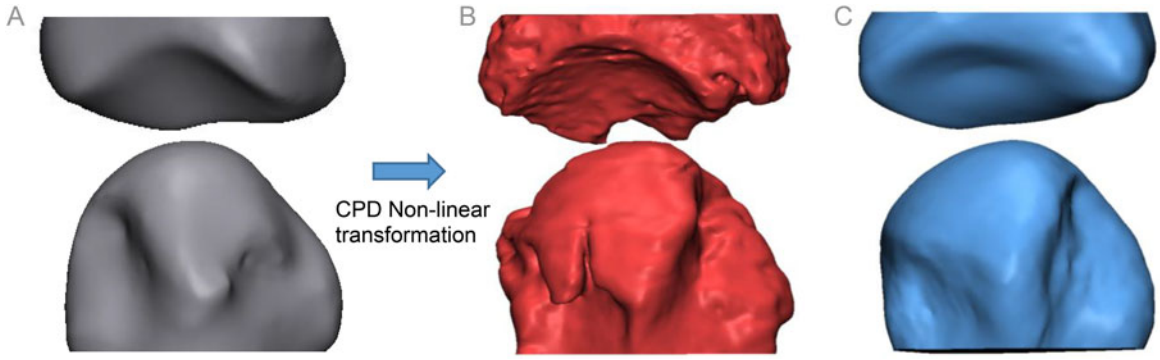

Figure 2. (A) The reference healthy surface is non-linearly transformed into the shape of the (B) diseased bone surface using CPD. The transformed surface is now considered the (C) estimated healthy surface of the original diseased surface.

2.2.3. Scaling and orienting surfaces

To define a common analysis region, all surfaces were equivalently proportioned based on bony landmarks. This served to reduce variability between subjects of different sizes by normalizing inter-subject bone volume and spatial position.

2.2.4. Creating a healthy reference surface

A single "generic" healthy reference surface was produced from the 12 healthy subject surfaces. Each healthy surface was characterized by M = 10,000 vertices (average vertex point-to-point resolution of 0.28 mm) positioned at corresponding anatomical locations. This allowed for a point-to-point correspondence between each n – {*number of healthy surfaces*} in the form of comparable point sets (Bookstein, 1997; Heimann et al., 2006; Bredbenner et al., 2014; Van Haver et al., 2014). This was carried out by mapping the dense, template point set $Y = (y_1, \ldots, y_M)$ in $\mathbb{R}^3$ to each healthy surface point set $X = (x_1, \ldots, x_n)$ using a non-rigid, modified Coherent Point Drift (CPD) transformation (Myronenko et al., 2007; Myronenko and Song, 2010). The CPD algorithm is a probabilistic Gaussian mixture model (GMM), non-rigid transformation technique used to register two dissimilar point sets (Yuille and Grzywacz, 1988; Myronenko et al., 2007). The result was a single healthy reference surface, generated by averaging the Euclidean space between all the corresponding transformed template point sets Y' to get a single average point set, such that:

Healthy Reference Surface $= \frac{\sum_{i=1}^{n} Y'_i}{n}$, where $i = 1, \ldots, n$.

2.2.5. Estimating healthy surfaces from diseased patient scans

To differentiate between healthy and diseased surfaces, the healthy reference surface was non-rigidly transformed to each patient surface mesh. The result was a new bone surface with healthy features that had similar size and geometry to the diseased surface. To accomplish this, a CPD algorithm was adapted to warp the reference healthy surface mesh (Figure 2A) into the shape of each patient specific diseased surface mesh (Figure 2B), while retaining the "healthy" features. This allowed prediction of the geometry of a patient healthy surface (Figure 2C) from the diseased surface.

2.2.6. Quantifying surface deformity

We characterized surface deformity as the deviation of the patient bone surface from the corresponding predicted healthy surface. A negative distance represented bone erosion while a positive distance represented periosteal bone growth (Figure 3). These distances, calculated over the entire surface, were used to develop outcome measures, described below.

- **Percentage surface area of periosteal bone growth and erosion (%):** The total bone surface area determined to be "diseased" (i.e., comprised of abnormal erosions or growths) was represented as a percentage of the total surface area. A threshold of 0.6 mm was selected based on a sensitivity analysis described in Section 3.3, where distances exceeding this threshold were considered "diseased". This outcome was further categorized into erosion and periosteal bone growth.
- **Number of independent erosion sites and bone growths**: The number of standalone erosion sites and periosteal bone growths were tallied for each surface.
- **Maximum positive and negative distance between surfaces (mm):** Maximum periosteal bone growth height (positive distance) and erosion depth (negative distance) were expressed in mm.

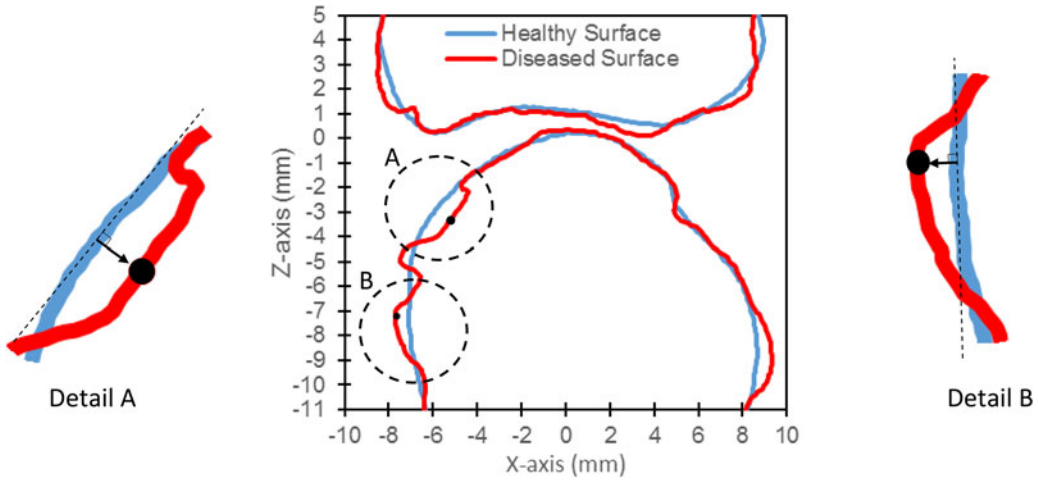

Figure 3. Cross-sectional profile of metacarpophalangeal joint with diseased surface (red) overlaid the corresponding predicted healthy surface (blue). In Detail A, the graphic illustrates a negative distance between the predicted healthy triangulated surface to the nearest diseased surface vertex in the normal direction of the respective triangle plane (erosion). Similarly, Detail B shows an example of a positive distance (periosteal bone formation).

2.3. Sensitivity analyses

The outcome measures depend on fitting an appropriate generic healthy surface to the diseased bone and then detecting differences between the two surfaces. We expected that even healthy joints would contain surface variations, due to age-related changes and biological variation. The goal of the sensitivity analyses were to (1) assess the degree to which our generic healthy surface was truly "generic", in the context of our small healthy subject sample, and (2) to systematically determine the minimum size for a feature to be considered "abnormal" that maximized algorithm sensitivity and specificity.

2.3.1. Making the generic healthy surface

To determine the degree to which the calculated parameters depended upon the specific reference surfaces used to generate the generic healthy surface, we conducted a sensitivity analysis using three randomly selected diseased surfaces. First, we determined how many healthy surfaces were required to create a generic healthy reference surface. To accomplish this, we quantified the maximum periosteal bone growth height for each diseased surface as the number of healthy surfaces used to create the generic surface increased from 2 to 12. Next, to determine the extent to which the *specific* healthy surfaces included within the generic surface affected the outcome measures, we selected 9 different combinations of 3 healthy surfaces to create different generic surfaces. These were each used to quantify the maximum periosteal bone growth height for each diseased surface.

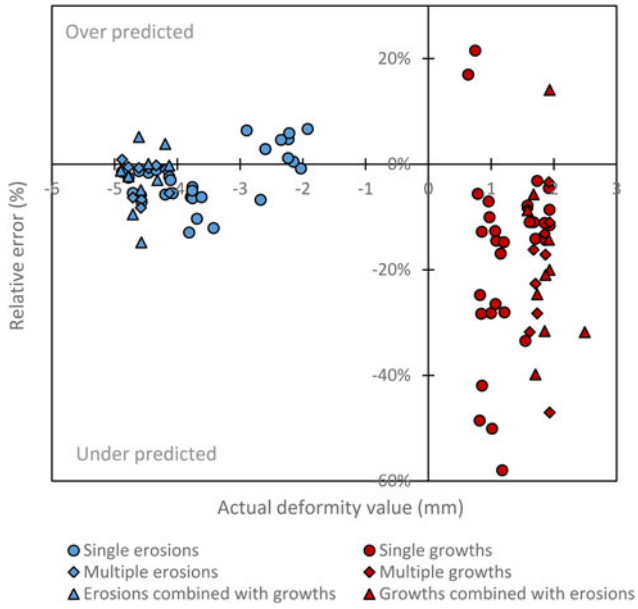

Figure 4. The relative error between the predicted values and the actual values of the deformity measurements represented as a percentage of the size of the deformity. Relative error = (predicted value – actual value)/actual value %. Erosion depths are illustrated in blue and periosteal bone growths in red.

2.3.2. Detection of erosions and periosteal growths

To quantify the accuracy and limitations of the algorithm, a series of artificial erosions and periosteal bone growths with known dimensions were manufactured on five different healthy surfaces. Algorithm-based measures were compared to the actual known values. Three sizes of erosion were constructed as 'U' shaped voids, and three sizes of periosteal growth were constructed as convex domes. Dimensions and shapes were selected based on clinical reports (Døhn

et al., 2007; Emond et al., 2012; Kocijan et al., 2014; Ventura-Rios et al., 2016; Ibrahim-Nasser et al., 2017). Erosions ranged from 1.9 to 4.9 mm in depth, and periosteal growths ranged from 0.6 to 1.9 mm in height. All types of artificial erosions and growths were placed individually and in combination on the healthy surfaces, resulting in 90 different simulations.

We assessed: (1) the ability to detect an erosion or growth, by systematically varying the cut-off threshold. This was the minimum distance between surfaces to be considered an erosion or growth and was determined from the average Youden's Index of the sensitivity and specificity plots. (2) The accuracy of erosion depth calculations. This was calculated as the root mean squared error (RMSE) of the measured versus actual depth or height. (3) The overall fit of the predicted healthy surface onto a given specific surface. Overall fit was expressed as the mean distance between the predicted and actual surface, in those regions without artificial erosions and growths.

2.4. Application to patient cohort

After determining the best performance parameters from the sensitivity analyses, the algorithm was applied to the healthy and patient cohorts. One way ANOVA was used to compare outcomes between groups. Post hoc t-tests with Bonferroni corrections were used to detect between-group differences. To determine the degree to which our outcome measures were associated with disease, stepwise discriminant analysis was used to blindly classify two mixed groups: 12 healthy plus 17 RA patients, and 12 healthy plus 17 PsA patients.

3. Results

3.1. Sensitivity analyses

3.1.1. Making the generic healthy surface

The surface matching algorithm was not very sensitive to either the number of surfaces used to create the generic healthy surface, nor the specific healthy surfaces used. When the number of surfaces used to create the generic healthy surface was increased from 2 to 12, maximum periosteal growth for the diseased surfaces varied $\leq$129 µm. Similarly, when different combinations of healthy surfaces were used to create the generic healthy surface, maximum periosteal growth varied $\leq$260 µm. Additional details are included in the supplemental data.

3.1.2. Detection of erosions and periosteal growths

A cut-off threshold of 0.6 mm was able to detect both erosions and periosteal growths with 87.5% sensitivity and 86.8% specificity. This was used for all subsequent calculations. Overall, the algorithm predicted erosion depth more accurately than periosteal bone growth height (Figure 4). Erosion depth RMSE was 4 ± 3% of the actual value, corresponding to an average precision error of 50 µm. The heights of periosteal bone growths were predicted to within 20 ± 13%, corresponding to an average precision error of 210 µm. Most deformities were slightly under-predicted. The algorithm was best at measuring deep, narrow erosions, and worst at measuring wide, gradual periosteal growths. Overall fit between surfaces was excellent, with an RMS distance of 0.08 mm between the generic-fitted surface and the non-modified portions of each healthy surface.

3.2. Application to patient cohort

The algorithm objectively illustrated areas of abnormal bone degradation and growth (Figure 5). In the metacarpal head, patients with PsA and RA had maximum positive distances (periosteal bone growth) that were $\geq$55% greater than the healthy cohort. Similarly, PsA and RA patients had maximum negative distances (erosions) for both the metacarpal head and phalangeal base that were >85% greater than the healthy cohort (Table 1).

Patients with PsA had significantly greater percentages of eroded bone surface area that compared to the healthy cohort (Table 1). The algorithm also detected significantly more erosion sites on the metacarpal head in both PsA and RA patients. Finally, the maximum depth of erosions was significantly greater in both the metacarpal head and phalangeal base of RA patients, and the phalangeal base of the PsA patients.

The outcome measures were able to discriminate healthy versus RA patients better than healthy versus PsA patients. At the metacarpal head, erosion depth and average surface matching successfully discriminated 96.6% of healthy and RA patient surfaces from each other (11/12 healthy and 17/17 RA surfaces). At the phalangeal base, a combination of erosion depth, periosteal growth height, percent surface eroded and surface variability correctly classified 100% of healthy and RA patient surfaces. At the metacarpal head of healthy and PsA patients, the number of erosion sites and average surface matching discriminated 86.2% correctly (12/12 healthy and 13/17 PsA surfaces).

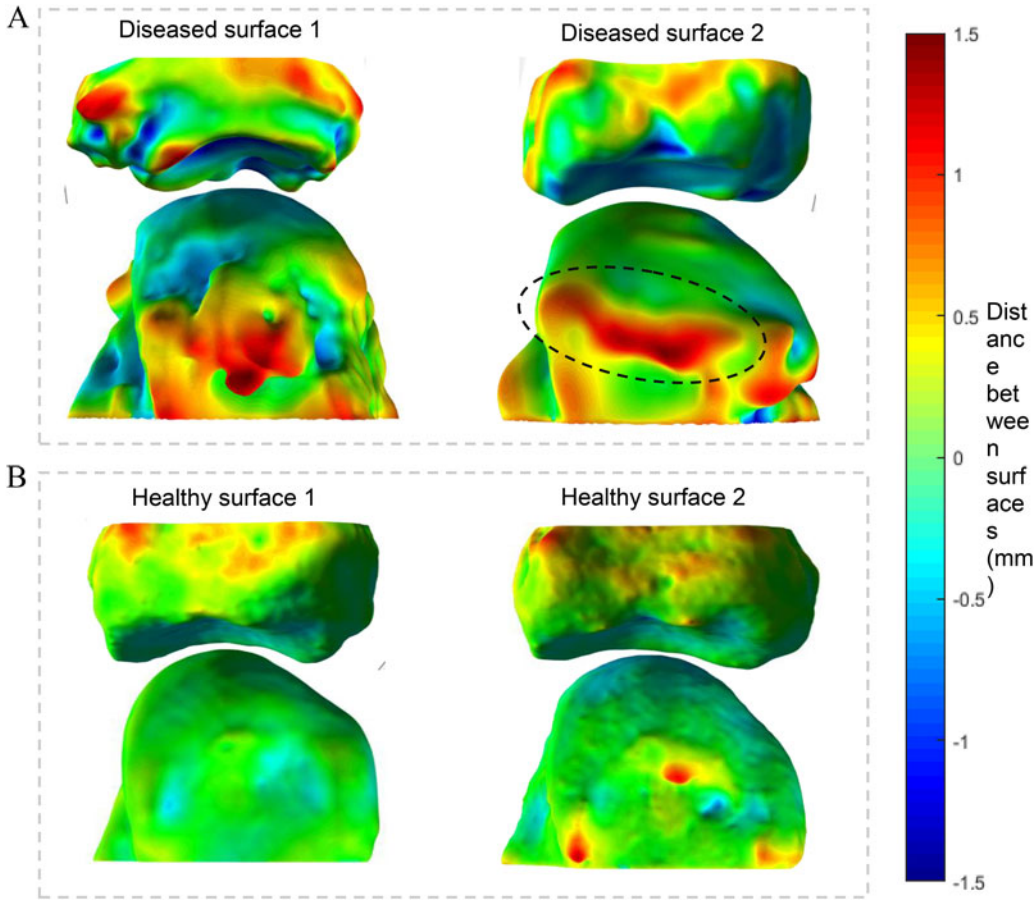

Figure 5. The visual outputs of the algorithm showing areas of erosion (blue) and periosteal bone growth (red). The heat map represents the distance between the subject bone surface and the corresponding predicted healthy surface. Two examples of diseased surfaces are illustrated in (A) and two examples of healthy surfaces in (B). The prevalence of erosion and bone growth is noticeably observable. The dashed ellipse in the top right panel illustrates a large ridge of abnormal periosteal growth.

However, at the phalangeal base, erosion depth alone was selected, which discriminated 72.4% of surfaces correctly (12/12 healthy and 9/17 PsA surfaces).

4. Discussion

Here, we developed an objective algorithm to quantify three-dimensional bone surface abnormalities based on HRpQCT images. The algorithm uses a generic healthy surface to predict the healthy surface topology of diseased bone. This allows for visualization and quantification of surface changes within the affected joint by defining areas of erosion and periosteal bone formation. We evaluated the sensitivity of these measures to input parameters, and compared sets of outcome measures in healthy subjects and patients with both RA and PsA.

Our data show that algorithm is not particularly sensitive to the number of, or specific healthy surfaces used to generate the generic healthy reference surface. Based on this data, and our assumption that including more healthy surfaces in the generic model would improve generalizability, all 12 healthy surfaces were used. Nevertheless, this number is relatively small compared to other population-based bone geometry atlases, and surface fitting may be improved by using age- or sex-specific references in the future. Algorithm performance accuracy and limitations were assessed by measuring artificial erosions and periosteal growths. Based on these data, a cut-off value of 0.6 mm was identified to best detect an unknown and mixed set of erosions and periosteal growths. The algorithm had difficulty in detecting and measuring periosteal bone growths because it is difficult to identify convex growths on an already convex bone surface. However, algorithm accurately identified erosion sites and growths adjacent to one another, which has clinical relevance especially in PsA patients. The sensitivity and specificity for detecting the presence of both erosions and periosteal growths in our test set was excellent (nearly 90%), and both features could be detected with an accuracy of 210 µm.

Table 1. Results comparing mean outcome measures of healthy subject surfaces to PsA diseased subject surfaces and RA diseased subject surfaces. Differences between PsA and RA surfaces are included. The outcome measures are reported as mean values ± standard deviation.

	Metacarpal results			Phalangeal base results		
Outcome measure	Healthy surface	PsA diseased surface	RA diseased surface	Healthy surface	PsA diseased surface	RA diseased surface
Mean distance between surfaces (mm)	−0.07 ± 0.04	−0.05 ± 0.07	−0.02 ± 0.06	−0.04 ± 0.03	−0.04 ± 0.04[a]	−0.01 ± 0.02[a,b]
Maximum positive distance between surfaces (mm)	0.60 ± 0.13	0.93 ± 0.45	0.94 ± 0.51	0.66 ± 0.05	0.87 ± 0.53	0.84 ± 0.36
Maximum Negative distance between surfaces (mm)	−0.71 ± 0.28	−1.31 ± 0.65	−1.62 ± 1.11[b]	−0.65 ± 0.05	−1.34 ± 0.68[b]	−1.44 ± 0.82[b]
Average Standard deviation of distances between surfaces (mm)	0.22 ± 0.05	−0.32 ± 0.17	0.28 ± 0.19	0.26 ± 0.03	0.30 ± 0.20	0.21 ± 0.10
Percentage surface area of periosteal bone growth (%)	0.1% ± 0.2%	3.8% ± 6.4%	1.5% ± 2.4%	0.4% ± 0.5%	3.0% ± 5.3%	1.2% ± 2.8%
Percentage surface area of erosions (%)	0.6% ± 1.2%	6.7% ± 8.7%[b]	2.8% ± 3.4%	0.2% ± 0.3%	4.9% ± 7.2%[b]	1.7% ± 3.2%
Number of independent erosion sites	0.8 ± 1.1	2.9 ± 2.7[b]	3.5 ± 3.9[b]	1.1 ± 0.8	1.9 ± 2.2[b]	1.9 ± 3.0
Number of independent bone growths	0.9 ± 1.0	4.5 ± 3.5	4.5 ± 4.4	0.7 ± 0.7	4.0 ± 3.5	2.4 ± 2.0

[a]Significant difference ($p < .05$) for outcome measures between **PsA** and **RA** diseased subject surfaces.
[b]Significant difference ($p < .05$) for outcome measures between **healthy** and **diseased** surfaces.

Several of the outcome measures have clinical relevance. Specifically, erosion depth was consistently and significantly greater in both patient groups compared to the healthy cohort. Other measures may also be important, although the present proof-of-concept study was not powered to detect smaller, but clinically relevant, differences. We found that a combination of erosion depth, number of erosion sites, periosteal growth height, percent surface eroded and surface variability could blindly discriminate between healthy and diseased bony surfaces. Based on these features, the algorithm was better able to discriminate RA than PsA versus healthy subjects. The present group of patients with PsA had bone surfaces that included a variable mix of erosions and abnormal periosteal growth, whereas the patients with RA had predominantly erosions. Surface area based outcomes are a novel way to interpret and further diagnose articular bone surfaces affected by PsA and RA. Further validation of these surface features, especially association with clinical markers of disease severity, is needed to fully understand their potential clinical relevance and utility.

The present algorithm compares the diseased surface to an estimated healthy surface to objectively quantify differences in surface morphology. This general approach is frequently used during surgical planning for unilateral deformities, in which the intact/healthy limb is imaged and mirrored onto the diseased/injured limb (Vlachopoulos et al., 2016). In the case of inflammatory arthritis, both hands may be affected and previous images may not be available. Here, we address this problem by predicting the geometry of a healthy bone surface from the geometry of the diseased bone surface. This healthy surface can serve many purposes in understanding disease progression and quantifying joint changes. Our algorithm does not require human intervention during the image registration process and is inherently an objective method to produce outcome measures. This technique could be used in conjunction with other published algorithms to initially detect bone abnormalities and define the original healthy surface topology for further analyses of the diseased geometry.

Using HRpQCT imaging, several groups have established metrics for quantifying cortical breaks (Töpfer et al., 2014; Peters et al., 2017; 2017), erosion depth (Töpfer et al., 2014; Barnabe et al., 2016) and volume (Töpfer et al., 2015) for individual erosions in patients with RA (Stach et al., 2010; Finzel et al., 2013; Paccou et al., 2014) and PsA (Ory et al., 2005; Kocijan et al., 2015). Our results support the relevance of these measures, since maximum erosion depth and periosteal growth height were discriminators between healthy and diseased surfaces. Defining erosions or periosteal bone growths covering large areas and that have complex geometries, has been a consistent challenge to this research (Figure 5). This highlights a limitation of using erosion site counts as a metric of bone destruction; it may be necessary to use the parameter in conjunction with other outcomes. Here, we identified and assessed the usefulness of several candidate measures that would represent the overall deformity of a bone surface. However, the point-to-point distances that are calculated with the

present algorithm could be used to calculate additional measures (e.g. spatial locations of specific features), which may have greater clinical relevance or serve as useful research tools.

Our work builds upon that of others to quantify periosteal growth for the first time, and to increase objectivity in defining diseased bone surface. Previously reported techniques analyze image data on a slice-by-slice basis (2D) and require human intervention to isolate erosion sites (e.g (Töpfer et al., 2014)). These methods have limitations related to subjective identification of erosion sites, the expertise required, and difficulty in analyzing severely deformed bones. Semi-automated methods generally require a smooth cortical surface surrounding the erosion site to detect a sharp change in the gray scale gradient (e.g (Duryea et al., 2008)). These methods work well in cases where erosions are sparse, obvious, and the erosion cavity is smooth with minimal fenestration into the trabecular region. However, on joint surfaces where erosions are not well defined, are numerous or are adjacent to periosteal bone formation, as in PsA, it becomes very difficult to place seeding points for pseudo-automated algorithms to detect these bone abnormalities. Our algorithm fills this critical gap by automating the detection of abnormal sites. Although the algorithm was validated using HRpQCT images in RA and PsA patients, HRpQCT remains primarily a research tool that is not widely available. It is likely that these methods can be adapted to detect bone surface abnormalities within other anatomic sites, populations, and using alternative 3 D imaging modalities (e.g. CT or MRI). In these cases, additional validation would be required to account for differences in feature size and imaging resolution.

Our proof-of-concept study has several limitations. First, we used a small sample of subjects to establish and tune the algorithm. Although the outcome measures calculated here were different between diseased and healthy groups, these specific measures may not be appropriate for all types of inflammatory arthritis and additional validation is needed. Second, our healthy control cohort was younger than the diseased cohort, and additional research is required to more robustly define appropriate healthy reference surfaces. It is likely that the specific values we identified for parameters such as cut-off values, sensitivity, and specificity for detecting features may require adjustment, once a large healthy reference database is obtained. Similarly, it may be necessary to adjust parameters for other anatomic locations, applications, or disease states. Unlike other work in this area, the present algorithm is presently limited to detecting surface features, and may not accurately quantify erosions that reside within the trabecular structure but have minimal cortical breaks. However, our algorithm was quite robust and demonstrated accuracy that was comparable to our scan resolution. Finally, the data reported here are cross-sectional in nature, and the degree to which progression of surface deformity can be measured over time is not known. Despite these limitations, our algorithm was able to successfully facilitate visualization of, and report objective metrics related to, bone surface deformity in individuals with RA and PsA.

In conclusion, we have developed and demonstrated a method for objectively detecting and quantifying surface feature abnormalities. This method automatically detects and measures various clinically relevant bony features, including those that previously could not be measured via human input or automated segmentation techniques. In our small pilot study, the method was able to detect significant differences between healthy and diseased groups, and was able to discriminate blindly between these groups. With further development and validation, this method may serve as a unique diagnostic tool for monitoring disease progression, or to detect small changes in joint surface in early disease. This algorithm will be useful by itself and in conjunction with current clinical techniques and research-based diagnostics for the evaluation of patients with RA and PsA.

Acknowledgements

The authors would like to thank Janice Weaver and Tatiana Held for their assistance in patient enrollment, and Mina Al-awquati for her assistance in subject assessment.

Declaration of interest

A patent application has been submitted by WPI based on these results.

Funding

This study was funded by a Collaborative Seed Grant from the University of Massachusetts Medical School and Worcester Polytechnic Institute.

References

Baillet A, Gaujoux-Viala C, Mouterde G, Pham T, Tebib J, Saraux A, Fautrel B, Cantagrel A, Le Loet X, Gaudin P, et al. 2011. Comparison of the efficacy of sonography,

magnetic resonance imaging and conventional radiography for the detection of bone erosions in rheumatoid arthritis patients: a systematic review and meta-analysis. Rheumatology (Oxford). 50(6):1137–1147.

Barnabe C, Toepfer D, Marotte H, Hauge E-M, Scharmga A, Kocijan R, Kraus S, Boutroy S, Schett G, Keller KK, et al. 2016. Definition for Rheumatoid Arthritis Erosions Imaged with High Resolution Peripheral Quantitative Computed Tomography and Interreader Reliability for Detection and Measurement. J Rheumatol. 43(10): 1935–1940.

Bookstein FL. 1997. Landmark methods for forms without landmarks: morphometrics of group differences in outline shape. Med Image Anal. 1(3):225–243.

Boutry N, Morel M, Flipo RM, Demondion X, Cotten A. 2007. Early rheumatoid arthritis: a review of MRI and sonographic findings. Am J Roentgenol. 189(6): 1502–1509.

Boyesen P, McQueen FM, Gandjbakhch F, Lillegraven S, Coates L, Wiell C, et al. 2011. The OMERACT psoriatic arthritis magnetic resonance imaging score (PsAMRIS) is reliable and sensitive to change: results from an OMERACT workshop. J Rheumatol. 38:2034–2038. http://www.jrheum.org/content/38/9/2034.abstract.

Bredbenner TL, Mason RL, Havill LM, Orwoll ES, Nicolella DP. 2014. Fracture risk predictions based on statistical shape and density modeling of the proximal femur. J Bone Miner Res. 29(9):2090–2100.

Burghardt AJ, Lee CH, Kuo D, Majumdar S, Imboden JB, Link TM, Li X. 2013. Quantitative in vivo HRpQCT imaging of 3D wrist and metacarpophalangeal joint space width in rheumatoid arthritis. Ann Biomed Eng. 41(12): 2553–2564.

Cantini F, Niccoli L, Nannini C, Kaloudi O, Bertoni M, Cassarà E. 2010. Psoriatic arthritis: a systematic review. Int J Rheum Dis. 13(4):300–317.

Cervinka T, Sievanen H, Lala D, Cheung AM, Giangregorio L, Hyttinen J. 2015. A new algorithm to improve assessment of cortical bone geometry in pQCT. Bone. 81: 721–730.

Døhn UM, Ejbjerg BJ, Hasselquist M, Narvestad E, Court -Payen M, Szkudlarek M. 2007. Rheumatoid arthritis bone erosion volumes on CT and MRI: reliability and correlations with erosion scores on CT, MRI and radiography. Annal Rheumatic Diseases. 66:1388–1392.

Duarte GV, Faillace C, Freire de Carvalho J. 2012. Psoriatic arthritis. Best Pract Res Clin Rheumatol. 26(1):147–156.

Duryea J, Magalnick M, Alli S, Yao L, Wilson M, Goldbach-Mansky R. 2008. Semiautomated three-dimensional segmentation software to quantify carpal bone volume changes on wrist CT scans for arthritis assessment. Med Phys. 35(6Part1):2321–2330. c:

Duryea J, Russell R, Gravallese EM, Kay J, Han R, Lu B, Solomon DH. 2016. Brief report: development and validation of a semiautomated method to measure erosion volume in inflammatory arthritis by computed tomography scanning. Arthritis. Rheumatol. 68(2):332–336.

Emond PD, Inglis D, Choi A, Tricta J, Adachi JD, Gordon CL. 2012. Volume measurement of bone erosions in magnetic resonance images of patients with rheumatoid arthritis. Magn Reson Med. 67(3):814–823.

Finzel S, Rech J, Kleyer A. 2013. Hochauflösende periphere quantitative CT (HRpQCT). Z Rheumatol. 72(2): 129–136.

Fouque-Aubert A, Boutroy S, Marotte H, Vilayphiou N, Bacchetta J, Miossec P, Delmas PD, Chapurlat RD. 2010. Assessment of hand bone loss in rheumatoid arthritis by high-resolution peripheral quantitative CT. Ann Rheum Dis. 69(9):1671–1676. http://ard.bmj.com/content/69/9/1671.abstract.

Frank RE. 1998. Psoriatic arthritis. J Insur Med. 30(4): 267–269.

Gladman DD. 2009. Psoriatic arthritis. Dermatol Ther. 22(1):40–55.

Gladman DD, Shuckett R, Russell ML, Thorne JC, Schachter RK. 1987. Psoriatic arthritis (PSA)-an analysis of 220 patients . Q J Med. 62(238):127–141.

Haavardsholm E, Østergaard M, Ejbjerg B, Kvan N, Uhlig T, Lilleas F, et al. 2005. Reliability and sensitivity to change of the OMERACT rheumatoid arthritis MRI score (RAMRIS) in a multi-reader longitudinal setting. Arthritis Rheum. 52:3860–3867.

Heimann T, Oguz I, Wolf I, Styner M, Meinzer H. 2006. Implementing the automatic generation of 3D statistical shape models with ITK. The Insight Journal, 2006; Jul MICCAI Open Science Workshop.

Huizinga T, Nigrovic P, Ruderman E, Schulze-Koops H. 2011. No overall progression and occasional repair of erosions despite persistent inflammation in adalimumab-treated rheumatoid arthritis patients: results from a longitudinal comparative MRI, ultrasonography, CT and radiography study - Commentary. Int J Adv Rheumatol. 9:68–69.

Ibrahim-Nasser N, Marotte H, Valery A, Salliot C, Toumi H, Lespessailles E. 2017. Precision and sources of variability in the assessment of rheumatoid arthritis erosions by HRpQCT. Joint Bone Spine. 85(2):211–217.

Kocijan R, Englbrecht M, Haschka J, Simon D, Kleyer A, Finzel S, Kraus S, Resch H, Muschitz C, Engelke K, et al. 2015. Quantitative and qualitative changes of bone in psoriasis and psoriatic arthritis patients. J Bone Miner Res. 30(10):1775–1783.

Kocijan R, Finzel S, Englbrecht M, Engelke K, Rech J, Schett G. 2014. Decreased quantity and quality of the periarticular and nonperiarticular bone in patients with rheumatoid arthritis: a cross-sectional HRpQCT study. J Bone Miner Res. 29(4):1005–1014.

McGonagle D, Tan AL, Tan AL. 2015. The enthesis in psoriatic arthritis. Clin Exp Rheumatol. 33(5 Suppl 96): S36–S39. http://www.ncbi.nlm.nih.gov/pubmed/26472070.

Myronenko A, Myronenko A, Song X, Song X, Carreira-Perpiñán MÁ, Carreira-Perpiñán MÁ. 2007. Non-rigid point set registration: coherent Point Drift. Adv Neural Inf Process Syst. 19:1009–1016.

Myronenko A, Song X. 2010. Point set registration: coherent point drift. IEEE Trans Pattern Anal Mach Intell. 32: 2262–2275.

Nishiyama KK, Shane E. 2013. Clinical imaging of bone microarchitecture with HRpQCT. Curr Osteoporos Rep. 11(2):147–155.

Ory PA, Gladman DD, Mease PJ. 2005. Psoriatic arthritis and imaging. Ann Rheum Dis. 64(Suppl 2):ii55–ii57.

Ostergaard M. 2005. An introduction to the EULAR-OMERACT rheumatoid arthritis MRI reference image atlas. Ann Rheum Dis. 64(suppl_1):i3–i7.

Østergaard M, McQUEEN F, Wiell C, Bird P, Bøyesen P, Ejbjerg BO, Peterfy C, Gandjbakhch F, Duer-Jensen A, Coates L, et al. 2009. The OMERACT psoriatic arthritis magnetic resonance imaging scoring system (PsAMRIS): definitions of key pathologies, suggested mri sequences, and preliminary scoring system for PsA hands. J Rheumatol. 36(8):1816–1824. http://www.jrheum.org/content/36/8/1816.abstract.

Paccou J, Edwards M, Moss C, Dennison E, Cooper C. 2014. High-resolution imaging of bone and joint architecture in rheumatoid arthritis. Br Med Bull. 112(1): 107–118.

Peters M, Scharmga A, de Jong J, van Tubergen A, Geusens P, Arts JJ, et al. 2017. An automated algorithm for the detection of cortical interruptions on high resolution peripheral quantitative computed tomography images of finger joints. PLoS ONE. 12: e0175829.

Peters M, Scharmga A, van Tubergen A, Arts J, Loeffen D, Weijers R, et al. 2017. The reliability of a semi-automated algorithm for detection of cortical interruptions in finger joints on high resolution CT compared to MicroCT. Calcif Tissue Int. 101(2):132–140.

Rahman P, Nguyen E, Cheung C, Schentag CT, Gladman DD. 2001. Comparison of radiological severity in psoriatic arthritis and rheumatoid arthritis. J Rheumatol. 28: 1041–1044. http://www.jrheum.org/content/28/5/1041.abstract.

SCANCO Medical. XtremeCT. 2017. http://www.scanco.ch/en/systems-solutions/clinical-microct/xtremect.html. [accessed 2017 5 Jan].

Schett G, Gravallese E. 2012. Bone erosion in rheumatoid arthritis: mechanisms, diagnosis and treatment. Nat Rev Rheumatol. 8(11):656–664.

Simon D, Faustini F, Englbrecht M, Kleyer A, Kocijan R, Haschka J. 2015. FRI0560 comparison of bone microstructure of psoriatic arthritis and psoriasis patients – an hrpqct study of anabolic and catabolic bone changes. Ann Rheum Dis. 74(Suppl 2):630. http://ard.bmj.com/content/74/Suppl_2/630.1.abstract.

Solomon DH, Kay J, Duryea J, Lu B, Bolster MB, Yood RA. 2017. Effects of teriparatide on joint erosions in rheumatoid arthritis: a randomized controlled trial. Arthritis Rheumatol (Hoboken, NJ). 69(9):1741–1750.

Stach CM, Bäuerle M, Englbrecht M, Kronke G, Engelke K, Manger B, Schett G. 2010. Periarticular bone structure in rheumatoid arthritis patients and healthy individuals assessed by high-resolution computed tomography. Arthritis Rheum. 62(2):330–339.

Töpfer D, Finzel S, Museyko O, Schett G, Engelke K. 2014. Segmentation and quantification of bone erosions in high-resolution peripheral quantitative computed tomography datasets of the metacarpophalangeal joints of patients with rheumatoid arthritis. Rheumatol (United Kingdom). 53:65–71.

Töpfer D, Gerner B, Finzel S, Kraus S, Museyko O, Schett G, Engelke K. 2015. Automated three-dimensional registration of high-resolution peripheral quantitative computed tomography data to quantify size and shape changes of arthritic bone erosions. Rheumatology (Oxford)). 54(12):2171–2180.

Van Haver A, De Roo K, De Beule M, Van Cauter S, Audenaert E, Claessens T, Verdonk P. 2014. Semi-automated landmark-based 3D analysis reveals new morphometric characteristics in the trochlear dysplastic femur. Knee Surg Sports Traumatol Arthrosc. 22(11):2698–2708. http://hdl.handle.net/1854/LU-4261344.

Ventura-Rios L, Hernandez-Diaz C, Sanchez-Bringas G, Madrigal-Santillan E, Morales-Gonzalez JA, Pineda C. 2016. A descriptive, cross-sectional study characterizing bone erosions in rheumatoid arthritis and gout by ultrasound. Clin Rheumatol. 35:2269–2276.

Vlachopoulos L, Dünner C, Gass T, Graf M, Goksel O, Gerber C, Székely G, Fürnstahl P. 2016. Computer algorithms for three-dimensional measurement of humeral anatomy: analysis of 140 paired humeri. J Shoulder Elb Surg. 25(2):e38–e48. doi:http://dx.doi.org/10.1016/j.jse.2015.07.027.

Yuille A. L, Grzywacz NM. 1988. The motion coherence theory. [1988 Proceedings] Second International Conference on Computer Vision. 344–353. Los Alamitos, CA: IEEE Computer Society Press.

Zayat AS, Ellegaard K, Conaghan PG, Terslev L, Hensor EMA, Freeston JE, et al. 2014. The specificity of ultrasound-detected bone erosions for rheumatoid arthritis. Ann Rheum Dis. 74(5):897–903. http://ard.bmj.com/content/early/2014/04/30/annrheumdis-2013-204864.abstract.